Earthquake Engineering, Tenth World Conference © 1992 Balkema, Rotterdam. ISBN 90 5410 060 5

Earthquake response of arbitrarily shaped structures in fluid

T. Nakamura & Y. Tanaka
Shinozuka Research Institute, Tokyo, Japan

Y. Motora
Taisei Corporation, Tokyo, Japan

ABSTRACT: The dynamic response of arbitrarily shaped offshore 3-D structures subjected to high-frequency horizontal ground excitations is investigated theoretically based on a Green's function approach. The motion of a structure is idealized as a lumped-mass model with multiple degrees of freedom, and the surrounding fluid is assumed to be linearly compressible and to undergo small-amplitude irrotational motion. The influence of three-dimensional solid geometry and fluid compressibility on the dynamic response is demonstrated for a tower-structure of elliptical cross-section.

1 INTRODUCTION

Concrete gravity-type oil production and storage platforms for deep water usually have huge multiple columns. Earthquake analysis of such offshore structures, such as a tripod tower for 300 m-deep water, requires special considerations due to the interactions between fluid and structure.

Several different solutions for earthquake-induced hydrodynamic pressure on flexible cylindrical towers of circular cross-section surrounded by a compressible fluid have been published. They include those by Liaw and Chopra (1974), Mei et al. (1979), Williams (1986), and Tanaka and Hudspeth (1988). The contribution of the fluid added mass to changes in the natural period of the structure and the significance of fluid compressibility have also been investigated. Liaw and Chopra (1975) and Kokkinowrochos and Tharos (1988) have obtained a solution for the hydrodynamic pressure on arbitrarily shaped bodies of revolution with a vertical axis. Goyal and Chopra (1989a, 1989b) have investigated the dynamics of axisymmetric intake/outlet towers of non-uniform cross-section, considering both foundation interaction effects and the influence of interior and exterior fluids which were considered incompressible. Recently, Williams (1991) obtained a solution for axisymmetric intake/outlet towers in which the influence of both interior and exterior compressible fluids was considered; appropriate Green's functions led to a pair of coupled line-integral equations. However, in the above studies no acceptable hydroelastic solutions have yet been developed for 3-D offshore structures with arbitrary geometrical shapes.

In this work, a new Green's function, a resolvent kernel, has been developed which already satisfies the seabed boundary condition, the free surface boundary condition, and the radiation condition. As a result, only the boundaries of fluid domains which are in contact with the structure need to be discretized. To treat the singular behavior of a Green's function, we have developed two kinds of function; one is derived by an eigenfunction expansion technique and the other is derived by a mirror image technique. Our adaptive method for treating singularities is different from the one adopted in surface-wave diffraction problems by Fenton (1978). Explicit results are presented for the hydrodynamic restoring force, the base shear force, dynamic displacement, etc., for an offshore tower of elliptical cross-section.

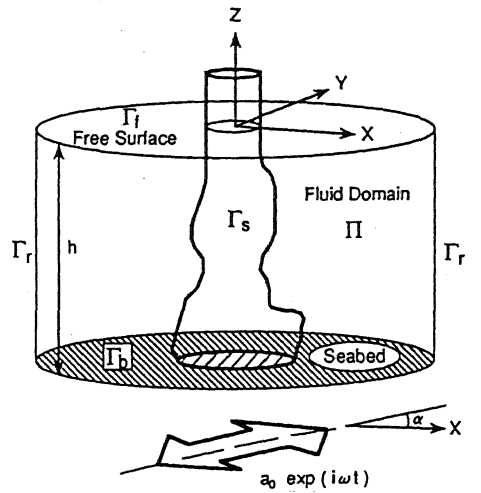

Figure 1. Definition sketch.

2 MATHEMATICAL FORMULATION

The fluid-structure system under consideration is shown in Fig. 1. An arbitrarily shaped structure is surrounded by water of uniform depth, h. The ground is subjected to horizontal motion of amplitude a_0 and frequency ω in a direction α from the x-axis, so $a(t) = a_0 \cdot \exp(i\omega t)$.

The fluid is assumed to be linearly compressible and its viscosity is negligible. The velocity potential $\Phi(\eta,y,z,t)$

can be separated into a stationary part, $\phi(x,y,z)$, and a time dependent part, $\exp(i\omega t)$; that is, $\phi(x,y,z,t) = \phi(x,y,z)\exp(i\omega t)$.

The small-amplitude, irrotational fluid motion is governed by the wave equation in Cartesian coordinate:

$$\nabla^2\phi + \frac{\omega^2}{c^2}\phi = 0 \qquad \text{in } \Pi \tag{1}$$

where c is the acoustic speed in water (c=1430 m/sec at 15°C) and ∇^2 denotes the 3-D Laplacian operator. The boundary conditions on $\phi(x,y,z)$ are

$$\phi = 0 \qquad \text{on } \Gamma_f \tag{2a}$$

$$\partial\phi/\partial z = 0 \qquad \text{on } \Gamma_b \tag{2b}$$

$$\partial\phi/\partial n = V_n \qquad \text{on } \Gamma_s \tag{2c}$$

where V_n denotes the normal velocity component of the body's surface and n is the unit normal inward the body. In addition, the potential $\phi(x,y,z)$ is required to satisfy the radiation condition at infinity

The motion of the structure is idealized as a lumped-mass model with three degrees of freedom, as shown in Fig. 2. The equation of motion for structure when acted on by fluid pressure may be written in the matrix form.

$$[M]\left(\{\ddot{d}\}-\{\ddot{a}\}\right)+[C]\left(\{\dot{d}\}-\{\dot{a}\}\right)+[K](\{d\}-\{a\}) = -[M]\{\ddot{a}\}-\{f\} \tag{3}$$

where [M] is the mass matrix, [C] is the structural damping matrix, [K] is the stiffness matrix, {d} is the absolute displacement vector of lumped mass, {a} is the ground displacement vector, and {f} is the vector of hydrodynamic restoring force acting on the lumped mass. Since the major horizontal displacements at each lumped mass are caused by bending deformation, since this is a tower-type structure, the equivalent shear spring constant in the stiffness matrix is determined from the beam stiffness. Vectors {d} and {a} are expressed in terms of each component of displacement.

$$\{d\} = \left\{d_{x1}, d_{y1}, \theta_{z1}, \ldots\ldots, d_{xm}, d_{ym}, \theta_{zm}\right\}^T e^{i\omega t} \tag{4}$$

$$\{a\} = \left\{a_x, a_y, o, \ldots\ldots, a_x, a_y, o\right\}^T e^{i\omega t} \tag{5}$$

where

$$a_x = a_0\cos\alpha\,;\; a_y = a_0\sin\alpha \tag{6}$$

Vector {f} is prescribed in terms of the restoring force due to hydrodynamic pressure.

$$\{f\} = \left\{f_{x1}, f_{y1}, f_{r1}, \ldots\ldots, f_{xm}, f_{ym}, f_{rm}\right\}^T e^{i\omega t} \tag{7}$$

A solution for the equation of motion, Eq. (3), is given by:

$$\{d\} = [A]^{-1}[B]\{a\} - [A]^{-1}\{f\} \tag{8}$$

where

$$[A] = -\omega^2[M] + i\omega[C] + [K] \tag{9}$$

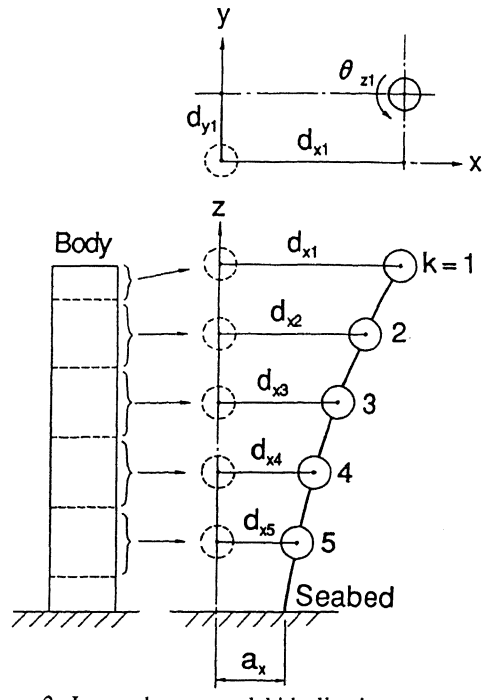

Figure 2. Lumped-mass model idealization.

$$[B] = i\omega[C] + [K] \tag{10}$$

when {f} is known in Eq. (8), the dynamic response {d} at each mass point of the structure can be determined. The components of restoring force at each mass point may be evaluated by integrating the hydrodynamic pressure, which is obtained by the linearized Bernoulli equation, over the surface area of the body $\Delta\Gamma_k$, as shown in Fig. 3.

$$\left\{f_{xk}, f_{yk}, f_{rk}\right\}^T = -i\omega\rho\int_{\Delta\Gamma k}\phi d\Gamma\left\{n_x, n_y, l_x n_y - l_y n_x\right\}^T \tag{11}$$

where ρ is the fluid mass density, n_x and n_y denote directional cosines with respect to the x and y axes, respectively, and l_x and l_y denote projected arm lengths in the x and y directions, respectively, from the twist center to the point on the body where the pressure acts. The motion of the body's surface can be described in terms of the displacement components, d_{xk}, d_{yk}, and θ_{zk}, associated with the lumped mass point k, as shown in Fig. 3. Therefore, the normal component of the body surface displacement at mass point k, Ψ_k, is expressed as:

$$\psi_k = \left[d_{xk}n_x + d_{yk}n_y + \theta_{zk}\left(l_x n_y - l_y n_x\right)\right]e^{i\omega t} \tag{12}$$

The time derivative of Ψ_k is equal to the normal velocity component of the body's surface V_n, at mass point k; thus, the kinematic boundary condition on the body's surface, as given by Eq. (2c), may be rewritten in the matrix form.

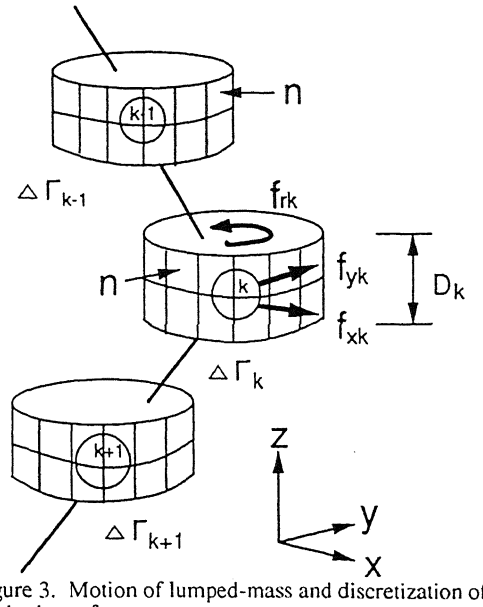

Figure 3. Motion of lumped-mass and discretization of the body surface.

$$\{\partial\phi/\partial n\} = i\omega[N]([A]^{-1}[B]\{a\} - [A]^{-1}\{f\}) \quad (13)$$

where $\{\partial\phi/\partial n\}$ denotes the normal velocity vector of the body's surface and [N] denotes the unit normal matrix defined in terms of n_x, n_y, and $(l_x n_y - l_y n_x)$.

3 SOLUTION BY INTEGRAL EQUATION APPROACH

The Green's function $G(x,y,z;\xi,\eta,\zeta)$ for the boundary value problem defined in Eqs. (1), (2a), and (2b) must satisfy

$$\nabla^2 G + \frac{\omega^2}{c^2} G = -\delta(x-\xi)(y-\eta)(z-\zeta) \quad \text{in } \Pi \quad (14)$$

$$G = 0 \qquad \text{on } \Gamma_f \quad (15a)$$

$$\partial G/\partial z = 0 \qquad \text{on } \Gamma_b \quad (15b)$$

where $\delta(\ )$ is the Dirac delta function. In addition, the Green's function is required to satisfy the appropriate radiation condition.

Applying the eigenfunction expansion method, we developed a suitable Green's function as

$$G(x,y,z;\xi,\eta,\zeta) = -\sum_{n=1}^{s} \frac{i}{2h} \sin k_n z \cdot \sin k_n \zeta \cdot H_0^{(2)}(\lambda_n R) + \sum_{n=s+1}^{\infty} \frac{1}{\pi h} \sin k_n z \cdot \sin k_n \zeta \cdot K_0(\lambda'_n R) \quad (16)$$

where $H_0^{(2)}$ is the zero-order Hankel function of the second kind, K_0 is the zero-order modified Bessel function of the second kind and

$$k_n = (2n-1)\pi/2h \,;\, n = 1,2,3,..... \quad (17a)$$

$$\lambda = \omega/c \quad (17b)$$

$$\lambda_n^2 = \lambda^2 - k_n^2 \quad ;n \le s \quad (17c)$$

$$\lambda_n^2 = k_n^2 - \lambda^2 \quad ;n > s \quad (17d)$$

$$R^2 = (x-\xi)^2 + (y-\eta)^2 \quad (17e)$$

where s is the largest integer satisfying the condition $[\lambda^2 - k_n^2] > 0$. Eq. (16) satisfies the radiation condition given by

$$\lim_{R\to\infty} \sqrt{R}\left(\frac{\partial G}{\partial R} + i\lambda_n G\right) = 0 \qquad \text{on } \Gamma_r \quad (18)$$

The effect of including the fluid compressibility is that two types of eigenmode appear in the Green's function; a propagating eigenmode for $\lambda^2 - k_n^2 > 0$ and an evanescent eigenmode for $\lambda^2 - k_n^2 < 0$. When the dimensionless frequency, $\Omega = 2\omega h/\pi c$, equals unity, the first cut-off frequency, ω, is given by $\omega = \pi c/2h$. It can be shown that at excitations below the first cut-off frequency there is no hydrodynamic radiation damping due to acoustic waves in the solution, only the added mass contributes to the hydrodynamic restoring force.

When R=0 in Eq. (16), the Green's function exhibits singular behavior. The fundamental solution satisfying the governing equation given by Eq. (14) is obtained by

$$G(x,y,z;\xi,\eta,\zeta) = \frac{1}{4\pi r} e^{-i\lambda r} \quad (19)$$

where

$$r^2 = (x-\xi)^2 + (y-\eta)^2 + (z-\xi)^2 \quad (20)$$

Equation (19) satisfies the radiation condition given by

$$\lim_{r\to\infty} r\left(\frac{\partial G}{\partial r} + i\lambda G\right) = 0 \qquad \text{on } \Gamma_r \quad (21)$$

In order to satisfy the bottom and free surface boundary conditions given by Eqs. (15a) and (15b), the mirror image technique is applied.

$$G = \frac{1}{4\pi}\left[\frac{e^{-i\lambda r}}{r} - \frac{e^{-i\lambda r_0}}{r_0} + \sum_{n=1}^{\infty}\left\{(-1)^n\left(\frac{e^{-i\lambda r_1}}{r_1} + \frac{e^{-i\lambda r_2}}{r_2}\right) + (-1)^{n+1}\left(\frac{e^{-i\lambda r_3}}{r_3} + \frac{e^{-i\lambda r_4}}{r_4}\right)\right\}\right] \quad (22)$$

where

$$r = \left\{(x-\xi)^2 + (y-\eta)^2 + (z-\zeta)^2\right\}^{1/2} \quad (23a)$$

$$r_0 = \left\{(x-\xi)^2 + (y-\eta)^2 + (z+\zeta)^2\right\}^{1/2} \quad (23b)$$

$$r_1 = \left\{(x-\xi)^2 + (y-\eta)^2 + (z-\zeta-2nh)^2\right\}^{1/2} \quad (23c)$$

$$r_2 = \left\{(x-\xi)^2 + (y-\eta)^2 + (z-\zeta+2nh)^2\right\}^{1/2} \quad (23d)$$

$$r_3 = \left\{(x-\xi)^2 + (y-\eta)^2 + (z+\zeta+2nh)^2\right\}^{1/2} \quad (23e)$$

$$r_4 = \left\{(x-\xi)^2 + (y-\eta)^2 + (z+\zeta-2nh)^2\right\}^{1/2} \quad (23f)$$

Applying Green's second identity to ϕ and G over the fluid domain, II, yields

$$\frac{1}{2}\phi(\xi,\eta,\zeta) = \int_{\Gamma_r}\left(\phi\frac{\partial G}{\partial n} - G\frac{\partial \phi}{\partial n}\right)d\Gamma \quad (24)$$

Equation (24) is a Fredholm integral equation for ϕ on the immersed body's surface. This integral equation may be solved numerically by discretizing the area of the integration into a number of small mesh elements.

The Green's function given by Eq. (16) has the property of rapid convergence; however singular behavior is exhibited when the point $P(\xi,\eta,\zeta)$ and the point Q (x,y,z) are close to each other. On the other hand, the Green's function given by Eq. (22) converges slowly, but it is possible to carry out integration even for the singular kernel. When $\lambda_n R>0.1$-0.3, the Green's function given by Eq. (16) is appropriate, while if $\lambda_n R<0.1$-0.3, Eq. (22) is better.

Once the values of ϕ on the body's surface have been determined, the dynamic response of the structure is obtained using Eq. (8). The total x-component of hydrodynamic restoring force F_{hx} may be obtained from

$$F_{hx} = -i\omega\rho\int_{\Gamma_r}\phi n_x d\Gamma \quad (25)$$

The base shear force of the structure F_{sx}, is given by

$$F_{sx} = F_{hx} - \omega^2\sum_{k=1}^{m} M_k(d_{xk} - a_x) \quad (26)$$

4 VERIFICATION OF THE NUMERICAL METHOD

To verify the numerical method presented here, several comparative calculations have been carried out on circular cylindrical structures.

The results given by the present method and the analytical solution by Tanaka and Hudspeth (1988) for the hydrodynamic restoring force acting on the rigid cylinder are composed in Fig. 4. Four values of the cylinder's radius/water depth ratio are investigated. In all cases, very satisfactory agreement with the numerical results is obtained. This comparison demonstrates that our new Green's functions are correct.

Figure 5 compares the numerical results and the analytical solution for total hydrodynamic restoring force and the base shear force on a flexible, squatty cylinder (r_0/h=0.25). The cylinder is idealized into a 10 discrete lumped-mass model and the circumference of the cylinder is discretized into 16 elements. The error in the 1st and 2nd mode natural frequencies in air is less than 1% when calculated by the lumped-mass model compared with the exact results obtained through continuous beam vibrations. The numerical results shown in Fig. 5 demonstrate good agreement with the eigenfunction solution.

Figure 6 illustrates the vertical distributions of the amplitude of the dimensionless horizontal dynamic response; the dimensionless added mass; and the dimensionless hydrodynamic radiation damping

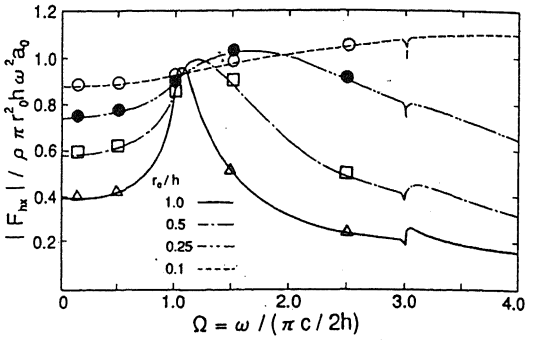

Figure 4. Total hydrodynamic restoring force on rigid cylinder.

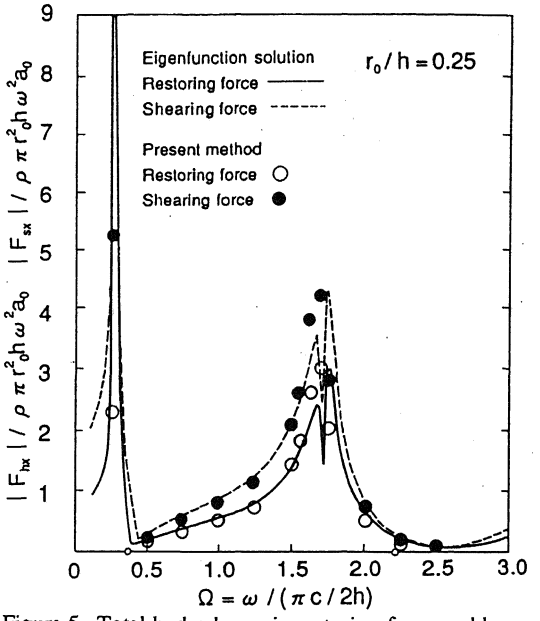

Figure 5. Total hydrodynamic restoring force and base shear force on flexible, squatty cylinder (r_0/h=0.25).

coefficient per unit length at the dimensionless frequency Ω=1.64. Again, the numerical results and the analytical solution are in good agreement.

5 NUMERICAL EXAMPLE

As an example, numerical results are presented here for a tower with an elliptic cross-section of which major-axis is 30 m and minor-axis is 24 m, a height of 100 m, and a wall thickness of 2 m. The structural data for this tower are listed in Table 1. The structural damping, C in Eq. (3), is taken to be zero. The tower structure is discretized into 16 lumped-mass nodes and the immersed surface is discretized into 17 (vertical) x 16 (circumferential) panels.

Figure 7 shows the dynamic displacement in the x and y directions at top of the tower, and the corresponding phase angle with dimensionless frequency Ω. Since the example tower is not a solid of revolution about the z

Table 1. Structural data for example tower.

		Major axis	Minor axis
Stiffness	(KN/m^2)	4.849×10^{11}	3.381×10^{11}
Mass distribution	(kg/m)	4.085×10^{5}	4.085×10^{5}
1st natural frequency in air:	(Hz)	1.928	1.610
2nd natural frequency in air:	(Hz)	12.08	10.09

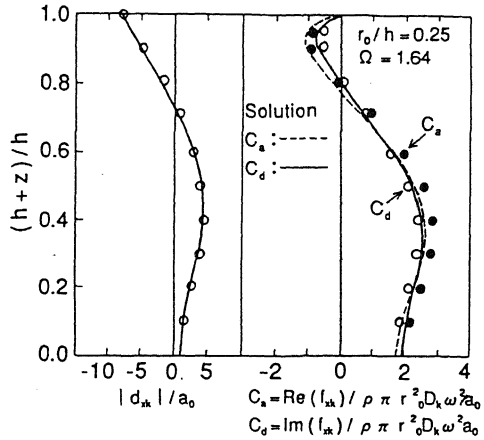

Figure 6. Added mass (C_a) and damping (C_d) coefficients per unit length and dynamic response for flexible squatty ($r_0/h=0.25$) flexible cylinder at $\Omega=1.64$.

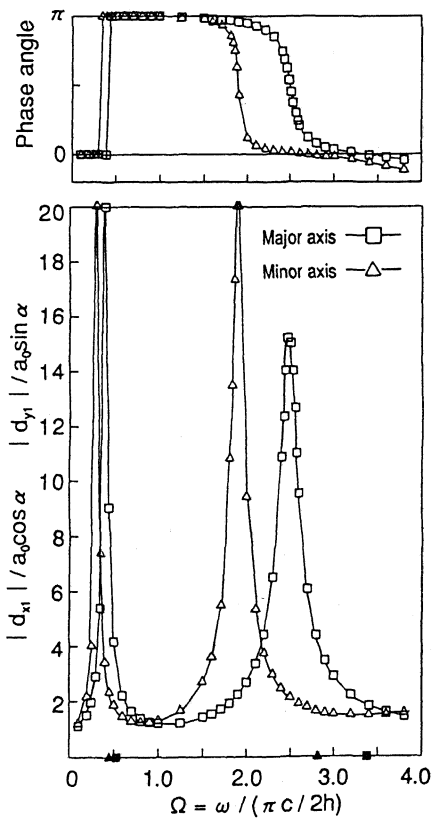

Figure 7 Dynamic displacement and phase angle of top lumped-mass node in x and y directions.

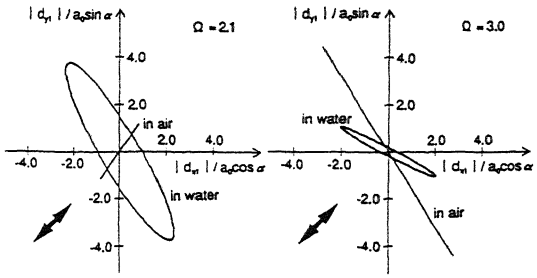

Figure 8. Trajectory of the dynamic motion of top lumped-mass node at $\Omega=2.1$ and $\Omega=3.0$.

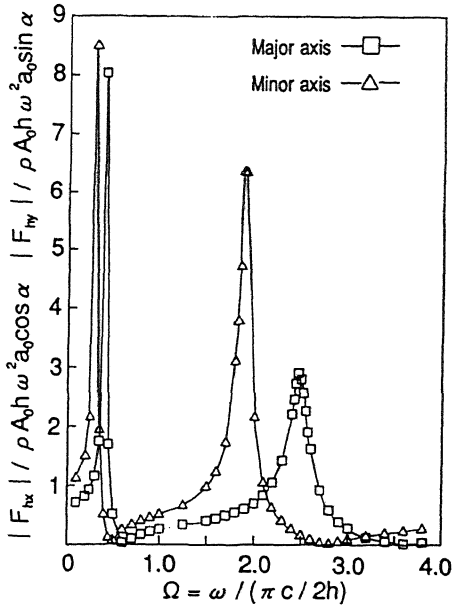

Figure 9. Total hydrodynamic restoring force in x (major axis) and y (minor axis) directions.

axis, the resonant frequency varies with horizontal direction. It is demonstrated that the hydrodynamic damping effects on the dynamic response amplitude near the 2nd natural frequency ($\Omega=1.5$-2.0). It should also be noted that the damping due to fluid compressibility is more effective in the x direction.

The trajectories of the dynamic motion at the top node for one excitation period are illustrated for dimensionless frequency $\Omega=2.1$ and $\Omega=3.0$ in Fig. 8. The direction of the ground excitation is taken to be $\alpha=45^{o}$; however the dynamic response of the top node demonstrates motion in different directions for $\Omega=2.1$ and $\Omega=3.0$. In addition, the trajectories form oval orbits. The reason for this is that the phase delays due to hydrodynamic damping are different for the major axis and minor axis. The trajectories of the dynamic movement at the same node when the tower is exposed in air, are also illustrated for reference. In this case, only reciprocating motion is observed because there is no hydrodynamic damping.

Figure 9 shows the hydrodynamic restoring forces in the x and y directions. From the comparison between

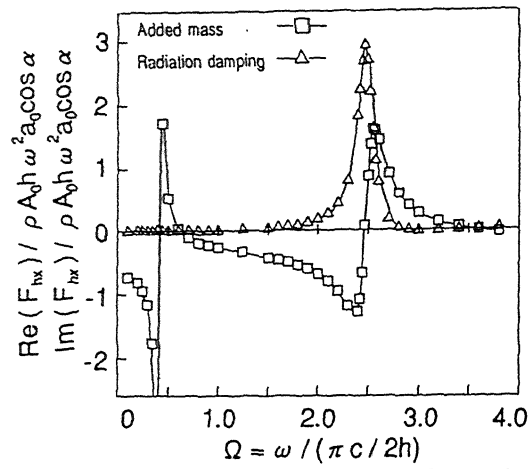

Figure 10. Total hydrodynamic added mass force and radiation damping force in x (major axis) direction.

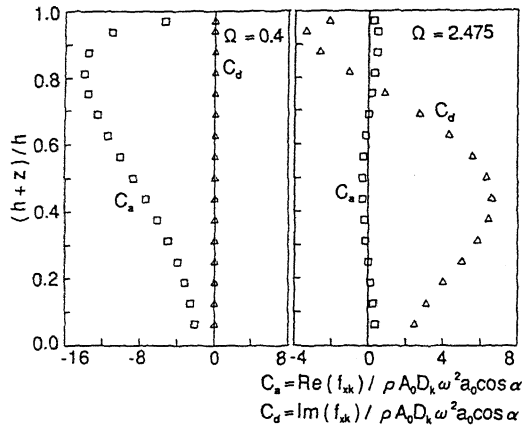

Figure 11. Vertical distribution of added mass (C_a) and damping (C_d) coefficients at Ω=0.4 and 2.475.

Fig. 7 and Fig. 9, it is observed that the hydrodynamic forces are strongly related to the dynamic motion of the body.

The hydrodynamic restoring force consists of two components: one in phase with the ground acceleration and another in phase with the ground velocity. Figure 10 shows the added mass term which is the real part of F_{hx} and the hydrodynamic damping term which is the imaginary part of F_{hx}. The hydrodynamic damping is dominant near the 2nd resonant frequency; and correspondingly, the added mass abruptly changes at this frequency. Figure 11 illustrates the vertical distribution of the added mass coefficient C_a and the radiation damping coefficient C_d per unit length for Ω=0.4 and 2.475. This comparison implies that the compressibility of the fluid is important at the 2nd resonant frequency.

6 CONCLUSION

The boundary integral equation method for the fluid domain and the lumped-mass method for the structural domain have been used to calculate the hydrodynamic force and associated dynamic response of an arbitrarily shaped 3-D offshore structure to horizontal ground excitations. Two new Green's functions have been developed to overcome singular behavior and to force quick convergence. The new Green's functions and the combined BEM and lumped-mass method have been verified by comparing numerical results with an analytical solution based on an eigenfunction expansion. Numerical results have been presented which illustrate the hydrodynamic restoring forces and dynamic response of a tower with an elliptical cross-section. Based on these numerical results, it is shown that consideration of the three-dimensional geometry of the tower is important; this is because the dynamic response of the tower traces oval loci due to hydrodynamic damping.

7 ACKNOWLEDGEMENTS

Special thanks are extended to Professor Robert T. Hudspeth Oregon State University, for providing invaluable help in the derivation of the Green's functions.

REFERENCES

Fenton, J.D. 1978. Wave forces on vertical bodies of revolution. *J. Fluid Mech.* 85(2): 241-255.

Goyal, A & A.K. Chopra 1989a. Earthquake analysis of intake-outlet towers including tower-water-foundation-soil interaction. *J. Earthquake Engng and Struct. Dyn.* 18(3): 325-344.

Goyal, A. & A.K. Chopra 1989b. Hydrodynamic and foundation interaction effects in dynamics of intake towers: frequency response function. *J. Struct. Div. ASCE*, 115(6): 1371-1385.

Kokkinowrachos, K. & I. Thanos 1988. Structure wave interaction under earthquake excitation. *Proc. 7th Int. Conf. OMAE*, Houston: 405-414.

Liaw, C.Y. & A.K. Chopra 1974. Dynamics of towers surrounded by water. *J. Earthquake Engng and Struct. Dyn.*, 3(1): 33-49.

Liaw, C.Y. & A.K. Chopra 1975. Earthquake analysis of axisymmetric towers partially submerged in water. *J. Earthquake Engng and Struct. Dyn.*, 3(3): 233-248

Mei, C.C., M.A. Foda & P. Tong 1979. Exact and hybrid element solutions for the vibration of a thin elastic structure on the sea-floor *Appl. Ocean Res.*, 1(2): 79-88.

Tanaka, Y. & R.T. Hudspeth 1988. Restoring forces of vertical circular cylinders forced by earthquakes. *J. Earthquake Engng and Struct. Dyn.* 16(1): 99-119.

Williams A.N. 1986. Earthquake response of submerged circular cylinder. *J. Ocean Engng.* 13(6): 569-585.

Williams A.N. 1991. Analysis of the base-excited response of intake-outlet towers by a Green's function approach. *J. Engng Struct.* 13(1): 43-53.